



Numerical Flow Analysis and Heat Transfer in Spirally Grooved Tubes in Heat Exchangers

Shamoon Jamshed¹ · Shafiq R. Qureshi¹ · Aqueel Shah¹

Received: 12 June 2017 / Accepted: 21 June 2018 / Published online: 28 June 2018
© Shiraz University 2018

Abstract

This paper deals with the heat transfer enhancement due to groove formation in a metallic tube. A detailed computational fluid dynamics (CFD) analysis was performed on helical groove tubes with three geometries (obtained from a published article) to validate the results, and three other geometries, randomly selected, with variable pitch length apart from experiment. The range of Reynolds number was from 4000 to 10,000. Performance criterion through CFD was based on the heat transfer via Nusselt number as well as the friction factor. The friction factor and Nusselt number comparison with experimental data was found to be in good agreement with the experimental data, with an average deviation of 2 and 7%, respectively. Numerical experimentation was extended by examining the performance of three more tubes of varying pitch lengths. The new tubes had pitch length of 51 mm (GT02), 102 mm (GT04) and 152 mm (GT06). The performance was evaluated in terms of thermal enhancement factor. It was found that the all tubes have enhancement factor greater than unity which means that tubes are efficient in terms of heat transfer. Among the tubes studied, the maximum thermal enhancement factor was also obtained for GT02 (51 mm pitch length).

Keywords Heat transfer · Computational fluid dynamics · Groove tubes · Nusselt number · Friction factor · Thermal enhancement factor

List of symbols

D_i	Internal diameter of the tube (m)
D_o	Outer diameter of the tube (m)
f	Friction factor (–)
g	Acceleration due to gravity (m^2/s)
h	Enthalpy (J/kg)
k	Turbulent kinetic energy (m^2/s^2)
L	Length of the tube (m)
\dot{m}	Mass flow rate (kg/s)
Nu	Nusselt number
Pr	Prandtl number
Re	Reynolds number
T	Temperature (K)
V	Velocity (m/s)
Δp	Pressure gradient (Pa/m)
q''	Heat flux (W/m^2)
y^+	Dimensionless wall normal distance

Greek letters

λ	Thermal conductivity (W/mK)
η	Thermal enhancement factor
μ	Absolute viscosity (kg/ms)
μ_t	Turbulent viscosity (kg/ms)
ρ	Density (kg/m^3)
ω	Specific dissipation rate (1/s)

Subscripts

avg	Average
f	Fluid
i	Internal
loc	Local
o	Outer
ref	Reference
w	Wall
t	Turbulent

✉ Shamoon Jamshed
shamoonjamshed@pnc.nust.edu.pk

¹ PNEC, National University of Sciences and Technology,
Karachi, Pakistan

1 Introduction

Heat transfer enhancement in heat exchangers has been the subject of much research for the past several decades. Technology advancement and new horizons in engineering in every era have compelled man to create complex structures. Thus, to enhance the efficiency and overall performance, heat exchangers are also under continuous improvement. It is evident in engineering that the performance of heat exchangers can be enhanced by increasing the surface area of the surface exposed to fluid. Finned surface designs are the most popular in this regard, Webb and Kim (2005). The work that has been done on enhanced-surface-tube research during the last century is mostly experimental based. In these studies, there is vast literature available enlightening the notable works of Webb and Kim and Kakaç et al. in texts like (2005; 1999). Webb et al. (1971) published a paper on the concept of repeated rib roughness. Correlations were established by him and found to be analogous to the results of experiments performed by the previous researchers like Nikuradse (1933), who did the research on plain pipe with sand-grain roughness. Webb concluded that his correlations were superior to other methods, particularly in the case of study of effect of Prandtl number. Jensen and Vlakancic (1999) studied the effect of fin height and depth within helical finned tubes. Reynolds number, based on the internal (finless) diameter of the tube, was from 10,000 to 90,000. The focus was to establish criteria for friction (f) and Nusselt number (Nu) at various fin heights. For small fin tubes, the friction factor curve experienced long transitional period before becoming fully turbulent at $Re = 20,000$. Webb et al. (2000) also discussed the heat transfer and friction in helical groove tubes, and the helical formation was made within the inner surface. Multiple regression correlation for Colburn j -factor ($StPr^{2/3}$) and friction factor were established. With the trend of correlations, the conclusion was that the tested tubes were successful in depicting the behavior of roughened surfaces (due to enhancement provided by local flow separation within the ribs). Gregory et al. (2008) conducted flow investigation in helically finned tubes and found heat transfer coefficients and friction factor in eight helically finned tubes and one smooth tube. The results, when compared with the results of experimental work by Webb et al. (2000), were well estimated within the prediction errors between 30 and 40%.

Grooved and finned geometries were also examined from numerical point of view. Liu and Jensen (2001) studied the effect of various fin profiles formed within a tube. The effects of height, number of fins, fin width and helix angle were numerically examined along with the

different shapes of fin profile. It was found that, for some geometric conditions, the performance variation is insignificant between rectangular and triangular fins, while for the round one, friction factors and Nusselt number were under-predicted (about 7–10%) than rectangular fins geometry. Kim et al. (2004a) also studied the fin geometries from a numerical perspective. A periodic portion was modeled to reduce the computational expense. A stable finite element method (SFEM) model technique was utilized to model the flow, and the problem was analyzed to see the fluid flow and heat transfer effects. Jasinski (2011) performed analysis using CFX code. Constant wall heat flux and fully developed 3D profile was applied as boundary condition. The influence of the helical angle of microfins on heat transfer and flow was examined. Effect of entropy generation with helix angle was also tested. Based upon the second law of thermodynamics and entropy generation rate minimization principle, it was found that minimum entropy generation rate appeared in the 70° helical tube and around Reynolds number of 60,000. Aroonrat et al. (2013) determined the Nusselt number and the friction factor for Reynolds number range from 4000 to 10,000. The effect of the most pronounced heat transfer was on Nu on tube with the largest helix angle (60°) with the least pitch of 0.5 inches. This behavior is also reflected in the friction factor curve. Recently, Pirbastami et al. (2016) compared the results with the findings of Aroonrat et al. (2013). The results were compared with $k - \omega$ model. A single groove, extruded into the length of the pipe helically, was considered for the analysis. There was a shortcoming of not considering the total number of starts (grooves appearing in cross section of the tube) in this study. It should be noted that it was not specifically mentioned in the Aroonrat paper that the single start (the groove/fin appearing in cross section) was taken, although a figure was mentioned with single start for explaining the nomenclature and all the grooves were not shown to avoid cluttering. Also, a table was mentioned for indicating number of starts for each grooved tube geometry. So as per the analysis of Pirbastami, it did not justify the fact that a single groove can be taken for CFD simulations and hence made the results of Pirbastami dubious.

Keeping the shortcomings in view of the above paper and to further augment the study of Aroonrat, the aim of this paper is to validate the results by Aroonrat for the following geometries, viz plain tube and two helical groove tubes. The results have been compared using CFD and with $k - \omega$ SST as turbulence model. It should be noted that a similar study by Jamshed et al. (2016) has been done, but with the purpose of validation with experiment only. Therefore, as a further research, three more helical groove tubes were analyzed in the analysis besides the experimental tubes to have a trend study in performance of the

tubes. The thermal enhancement factor has also been discussed for these tubes.

2 Experimental Setup for CFD Validation and Tube Geometries

The tube geometries were selected from the experiment that was performed by Aroonrat et al. (2013). In the experiment, a number of tubes with variable helix angles were used. The tube was 2 m in length and was made of Steel MS 304. T-type thermocouples were flush mounted to compute the temperature at the test section ends and also along the length of the test section (see Fig. 1). Working fluid was water with the inlet temperature of 25 °C. Pressure transducer was mounted across the length of the test section to measure pressure drop, while the test section was heated uniformly with DC power supply to provide constant heat flux condition. The groove tube terminology is embedded in the sketch of Fig. 2. It should be noted that a single groove is shown for clarity. The test section in the experiment was tested with a number of tubes, namely the simple metallic tube (SMT) and two helical groove tubes with alternating pitches. The tubes are named using convention ‘GTXX,’ where ‘GT’ indicates grooved tube and ‘XX’ denotes the axial pitch of the grooves in inches. The geometric details of the tubes with important parameters and those which were studied apart are both mentioned in Table 1.

3 Mathematical Modeling

3.1 Governing Equations

The phenomenon under consideration is based on the steady-state equations of the continuity, the time-averaged incompressible Navier–Stokes equations and the energy equation. These are mentioned below in their differential form as:

$$\frac{\partial \rho}{\partial t} + \nabla \cdot (\rho \bar{V}) = 0 \tag{1}$$

$$\begin{aligned} \frac{\partial(\rho V)}{\partial t} + \nabla \cdot (\rho \bar{V} \times \bar{V}) = & -\nabla p + \nabla \\ & \cdot \mu_t \left(\nabla \bar{V} + (\nabla \bar{V})^T - \frac{2}{3} \delta(\nabla \cdot \bar{V}) \right) \\ & + (\rho - \rho_{ref})g \end{aligned} \tag{2}$$

and

$$\begin{aligned} \frac{\partial(\rho h_{tot})}{\partial t} = & \frac{\partial \rho}{\partial t} + \nabla \cdot (\rho \bar{V} \times h_{tot}) \\ = & \nabla \cdot (\lambda \nabla T) + \nabla \cdot (\bar{V} \tau_w) + S_E \end{aligned} \tag{3}$$

3.1.1 The $k - \omega$ Turbulence Model

To solve the turbulent flow quantities, the $k - \omega$ shear stress transport (SST) model was used. The robust model was selected since it incorporates the k model outside the boundary layer and $k - \omega$ standard within the boundary layer. The only requirement for using this model is that the y^+ value should be ≤ 1 in the viscous sub-layer region of the turbulent boundary layer (see Ref ANSYS Incorporated 2016).

The $k - \omega$ SST model in its mathematical form is described below. The turbulent kinetic energy rate is given by:

$$\frac{\partial k}{\partial t} + U_j \frac{\partial k}{\partial x_j} = P_k - \beta * k\omega + \frac{\partial}{\partial x_j} \left[(v + \sigma_k v_T) \frac{\partial k}{\partial x_j} \right] \tag{4}$$

where P_k (the production limiter) is defined as:

$$P_k = \min \left(\tau_{ij} \frac{\partial U_i}{\partial x_j}, 10\beta^* k\omega \right) \tag{5}$$

and the specific dissipation rate is given as:

$$\begin{aligned} \frac{\partial \omega}{\partial t} + U_j \frac{\partial \omega}{\partial x_j} = & \alpha S^2 - \beta \omega^2 + \frac{\partial}{\partial x_j} \left[(v + \sigma_\omega v_T) \frac{\partial \omega}{\partial x_j} \right] \\ & + 2(1 - F_1) \sigma_{\omega 2} \frac{1}{\omega} \frac{\partial k}{\partial x_i} \frac{\partial \omega}{\partial x_j} \end{aligned} \tag{6}$$

Fig. 1 Schematic of the tube length and the position of thermocouples used in experiment are marked (Aroonrat et al. 2013)

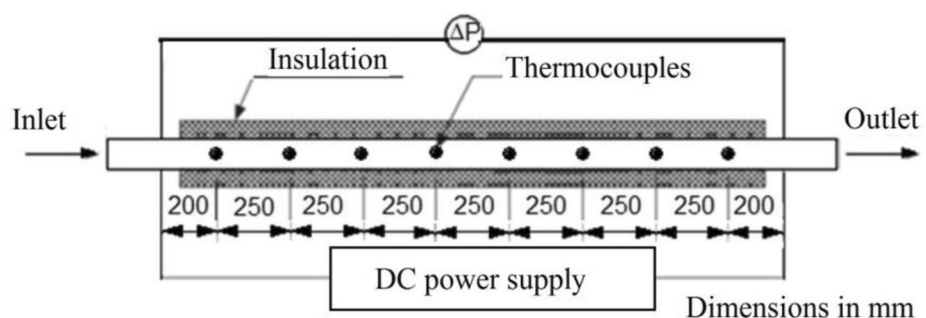


Fig. 2 The sketch of the groove tube geometry showing two views and nomenclature

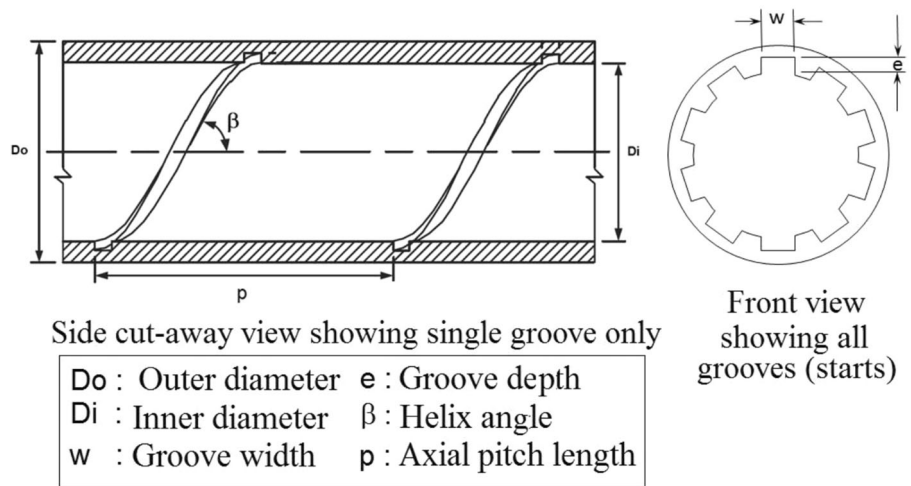


Table 1 Dimensional details of all the groove tubes analyzed

Tube	β (°)	Pitch (in)	Pitch (mm)	Remarks
GT08	6.3	8	203.2	Experiment
GT10	5	10	254	Experiment
GT02	23.6	2	51	Current study
GT04	12.3	4	102	Current study
GT06	8.3	6	152	Current study

The turbulent viscosity, which is an essence of all the RANS-based models, is defined as:

$$\mu_t = \nu_t \rho = \frac{a_1 k}{\max(a_1 \omega, SF_2)} \rho \tag{7}$$

where S is an invariant measure of the strain rate and a_1 is a constant of the model. In the equations of the specific dissipation rate Eq. (6) and turbulent viscosity Eq. (7), the terms F_1 and F_2 were defined. These terms are the blending functions. It should be noted that $F_1 = 1$ within the boundary layer and zero outside of it. Thus, it ‘switches’ (selects) a suitable turbulence model ($k - \omega$ standard or

$k - \epsilon$) during calculations. All the constants are defined in Table 2.

$$F_1 = \tanh \left\{ \left\{ \min \left[\max \left(\frac{\sqrt{k}}{\beta * \omega y}, \frac{500\nu}{y^2 \omega} \right), \frac{4\sigma_{\omega 2} k}{CD_{k\omega} y^2} \right] \right\}^4 \right\} \tag{8}$$

and

$$F_2 = \tanh \left[\left[\max \left(\frac{2\sqrt{k}}{\beta * \omega y}, \frac{500\nu}{y^2 \omega} \right) \right]^2 \right] \tag{9}$$

3.2 Data Reduction from Simulations

The performance was mainly evaluated on the basis of friction factor, averaged heat transfer coefficient, the Nusselt number and the thermal enhancement factor as given in Eqs. 10 through 13.

$$f = \Delta p D_i / (L 0.5 \rho V^2) \tag{10}$$

where Δp is the pressure drop along the length of the tube.

$$h_{avg} = \frac{\dot{Q}}{A_i (T_{avg,wi} - T_{avg,f})} \tag{11}$$

\dot{Q} is the power applied to the outer wall. A_i is the inner tube surface area, $T_{avg,wi}$ is the average temperature of the inner wall, and $T_{avg,f}$ is the bulk average temperature of water computed using the average of inlet and outlet temperature.

The Nusselt number was computed using the formula:

$$Nu = \frac{h_{avg} D_i}{\lambda_f} \tag{12}$$

For determining the heat enhancement for different tubes, a factor called the thermal enhancement factor was calculated using the following relation:

Table 2 Constants for the $k - \omega$ SST turbulence model

Constants	Value
α_1	0.556
α_2	0.44
β_1	0.075
β_2	0.0828
β^*	0.09
σ_{k1}	0.85
σ_{k2}	1
$\sigma_{\omega 1}$	0.5
$\sigma_{\omega 2}$	0.856

$$\eta = \frac{Nu/Nu_s}{f/f_s} \quad (13)$$

The subscript 's' is for smooth tube. This term helps in determining the effective heat transfer performance for grooved tubes. A value greater than unity in the above equation shows that the design of the tube is beneficial in terms of heat transfer enhancement.

3.3 Grid Independence Study

The grid independence study was done on simple tube geometry. Six cases were simulated on axi-symmetric tube whose mesh detail is mentioned in Table 3. For each case, the mesh was clustered near the walls to resolve the boundary layer gradients adequately. The first cell height was with respect to $y^+ \leq 1$.

For grid convergence monitoring, the axial velocity profile was examined as shown in Fig. 3. It was found that after three levels of mesh refinement, the velocity profiles showed less than 1% variation at the point of maximum velocity, which is at the center of the tube. All cases were run at the maximum Reynolds number of 10,000. Mesh level V was selected for validation with experimental data.

3.4 Grid Generation for Helical Groove Tube

Two grooved tubes mentioned in the Aroonrat paper were analyzed using CFD. Both the tubes had the same outer diameter of 9.5 mm and the inner diameter of 7.1 mm. Helix angle was 8° and 10° (measured with reference to the central axis). The number of starts (grooves appearing in cross section of the tube) was 10. The mesh was created with a technique similar to what was mentioned in the literature such as by Kim et al. (2004a, b; Liu and Jensen 2001; Jasinski 2011). A sector consisted of a 36° segment was constructed by taking advantage of periodic flow conditions. There were solid and fluid zones sharing an interface region between them as shown in Fig. 4.

Table 3 Mesh level details for grid convergence study

Mesh level	Number of cells	First near-wall cell size (mm)
I	6487	0.13
II	12,475	0.01
III	17,465	0.01
IV	24,451	0.001
V	30,083	0.001
VI	49,390	0.001

3.5 Numerical Method Employed and Boundary Conditions

The SIMPLE algorithm of Patankar (1980) was applied for solving pressure and velocity equations. SIMPLE stands for Semi-Implicit Pressure Linked Equations. All the basic quantities, namely pressure, velocity, turbulence scalar quantities and energy, were solved using second-order upwind scheme. The gradients were resolved using the least square cell-based scheme.

Convergence was monitored for residuals of equations of continuity, x , y and z velocities, turbulence quantities and energy. Further, the convergence for pressure drop and velocity at outlet was monitored when there was no change in their magnitudes for at least a hundred iterations. Mass imbalance between velocity inlet and pressure outlet was also confirmed to be zero for numerical consistency. All the cases were run on 4 cores of Intel Core *i7* eight core processor with 16 Gb RAM. Each Reynolds number case took around 8 h with convergence in about 14–15 k iterations.

3.5.1 Boundary Conditions

The boundary conditions were assigned in the solver. The solver used in this study case was ANSYS Fluent v16. The fluid was liquid water, whose physical properties were taken at the same temperature as the experiment that was performed, i.e., 298.15 K. The properties of steel MS 304 were also taken at the same temperature. Uniform velocity was input at the inlet, and the turbulent intensity was computed using the guideline from Fluent user guide (ANSYS Incorporated 2016). It was computed using the following formula:

$$\text{Turbulent intensity} = 16Re_D^{-1/8} \quad (14)$$

Heat flux of 3500 W/m^2 was applied on the outer tube surface, as per given in the reference Aroonrat et al. (2013), while interface was created between the solid and fluid junctions.

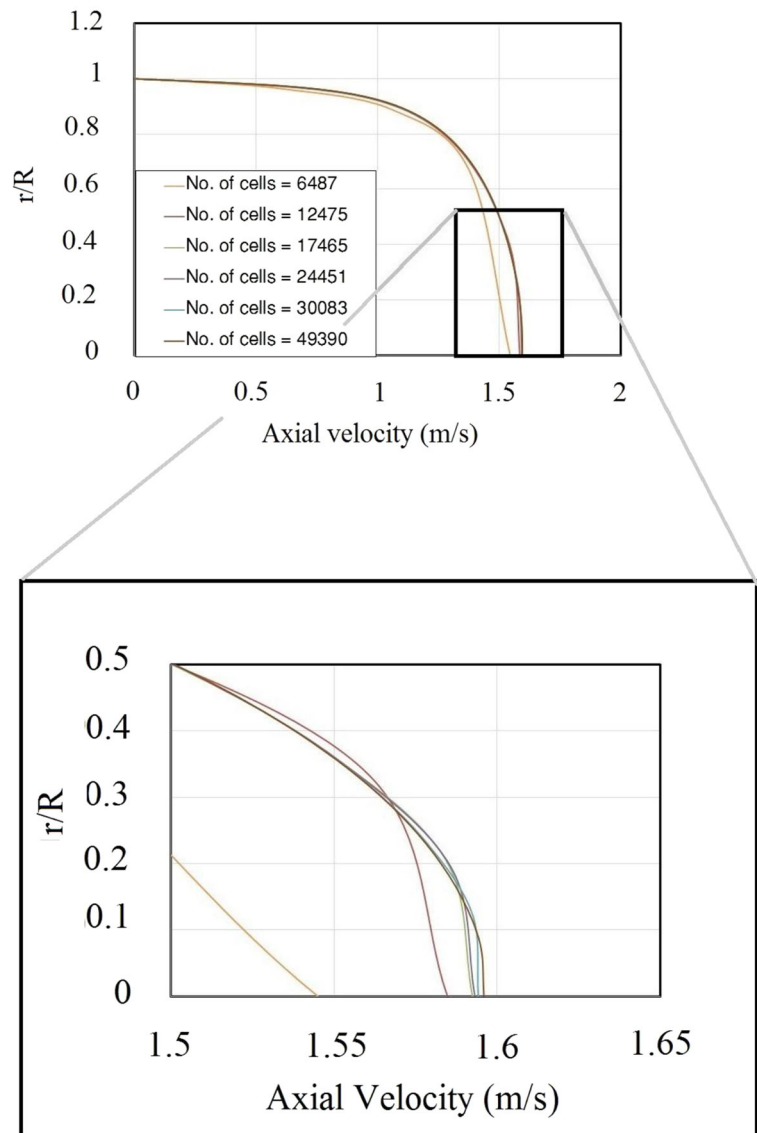
4 Results and Discussion

4.1 Validation with Experimental Data

4.1.1 Simple Metallic Tube (SMT) Results

For heat transfer enhancement analysis, the overall performance can be examined by considering the effect of both fluid dynamics and heat transfer. Thus, friction factor and Nusselt number were evaluated for simple metallic

Fig. 3 Grid convergence study for axial velocity profiles



tube (SMT), and then, its performance with experimental data was compared as shown in Figs. 5 and 6. It can be seen that CFD results are in good agreement with experiment, with average error (average over range of Reynolds number) of about 1% for friction and 6% for Nusselt number. The Nusselt number results also lie within the uncertainty limit of $\pm 18\%$ of the experiment. Moreover, in Fig. 5, the comparison of friction factor was also done with the theoretical functions. They are Blasius (1913) and Colebrook (1939) and are mentioned in Eqs. 15 and 16, respectively. The trends of the present work are similar to these equations.

$$f = 0.316Re^{-1/4} \quad (15)$$

and

$$\frac{1}{\sqrt{f}} = -2 \log \left(\left(\frac{\epsilon}{D_i} \right) + \frac{2.5}{Re\sqrt{f}} \right) \quad (16)$$

4.1.2 Validation of Helical Groove Tubes with 203 and 254 mm Pitch Length (GT08 and GT10)

The helical tubes' performance was tested with the comparison of friction factor as well as Nusselt number. This is shown in Figs. 7, 8, 9 and 10. It can be seen that the average error (over Re range) is within 2% for all the test cases for friction and it is in acceptable range. The comparison of Nusselt number curves obtained through CFD simulation with the experiment also shows that the difference is very low (about 7% on average over Re range) between CFD and experimental data and lies within the uncertainty limit of $\pm 18\%$ of experimental data. By satisfactory agreement

Fig. 4 Three-dimensional grid view of helical grooved tube geometry with mesh details in subfigure

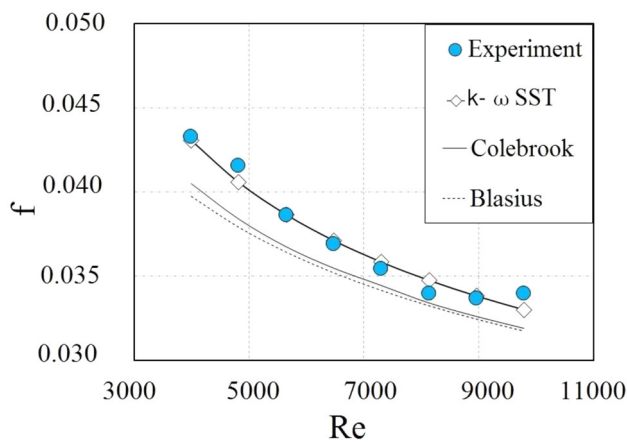
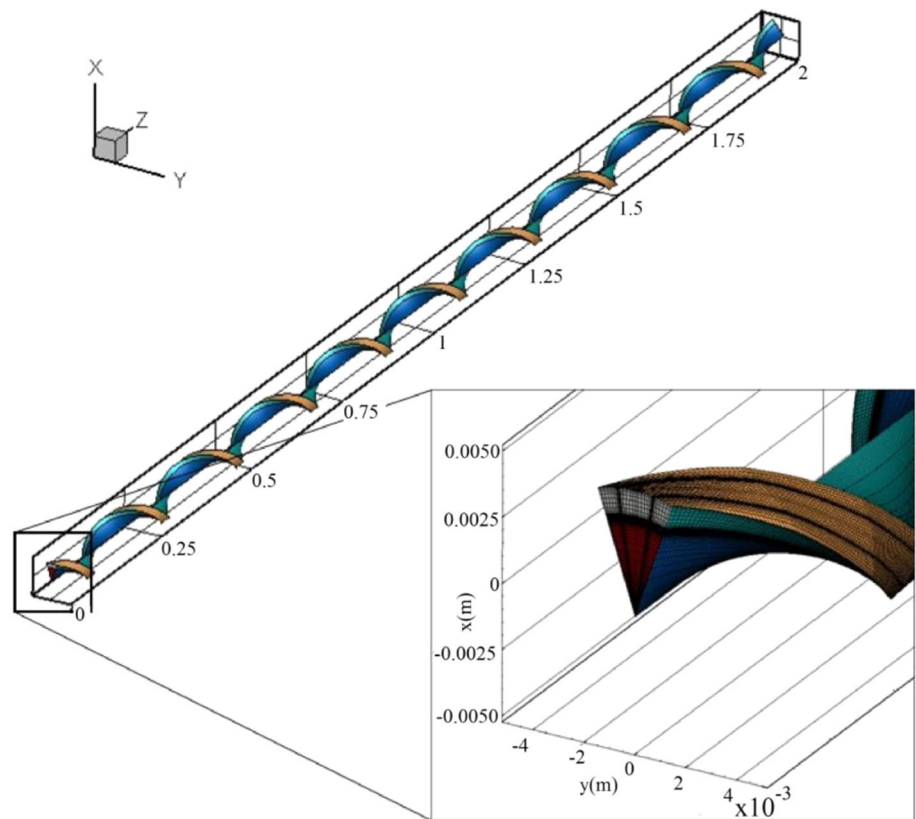


Fig. 5 Comparison of straight tube results for friction factor with $k - \omega$ SST model as well as Colebrook and Blasius equations

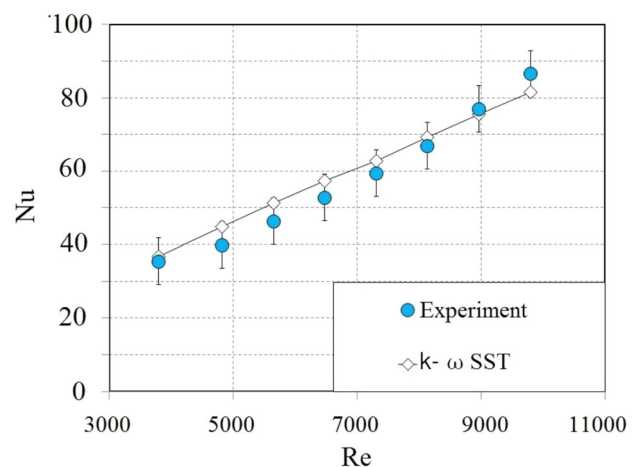


Fig. 6 Comparison of straight tube results for Nusselt number with $k - \omega$ SST model

with the experimental data, it can be said that the CFD can be used to analyze the results of other configurations, particularly by varying pitch lengths of the helical groove tube.

4.2 Performance of Tubes with 51, 102 and 152 mm Pitch Length (GT02, GT04 and GT06)

The objective was to obtain overall performance with analysis from low to higher pitches, as well as to see the

trend of performance parameters with regard to range of varying helix angles. Thus, in order to study the effect of variation in pitch length (particularly lower pitch length) on performance parameters, three more tubes were analyzed. The detail of the new tubes is given in Table 4.

Figure 11 reveals the friction factor plots for grooved tube geometries. These are also compared with smooth tube. The friction factor curves do not differ much when they are compared with smooth tube friction factor. Also,

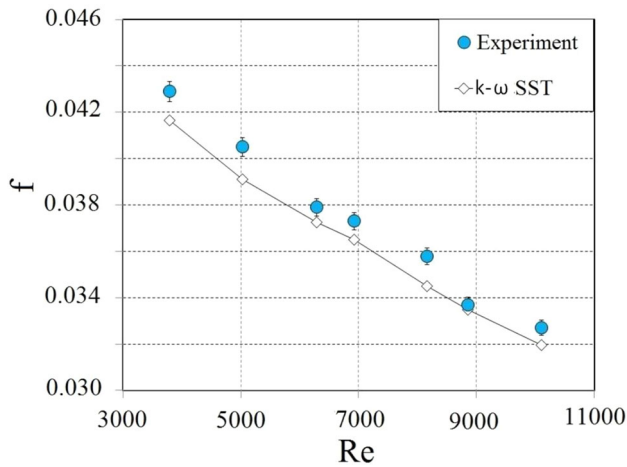


Fig. 7 Comparison of friction factor with experimental data as a function of Reynolds number for GT08 (203 mm pitch length)

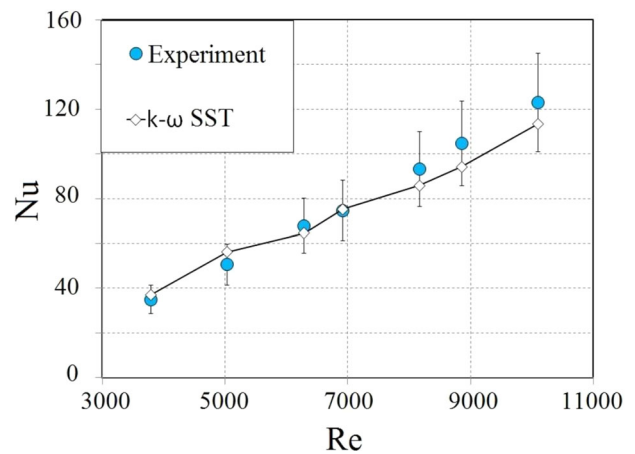


Fig. 10 Comparison of Nusselt number with experimental data as a function of Reynolds number for GT10 (254 mm pitch length)

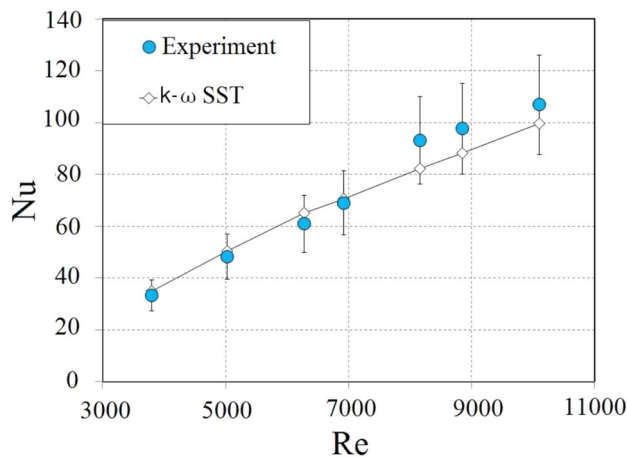


Fig. 8 Comparison of Nusselt number with experimental data as a function of Reynolds number for GT08 (203 mm pitch length)

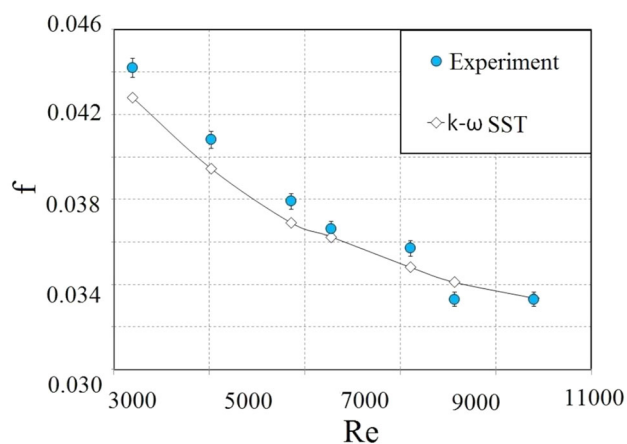


Fig. 9 Comparison of friction factor with experimental data as a function of Reynolds number for GT10 (254 mm pitch length)

the highest friction factor has been observed with GT02, showing an average difference of about 4%, in the Re range tested, with smooth tube. The maximum friction factor for GT02 was found to be 5% from smooth tube. Figure 12 shows the Nusselt number curves for three different helical tubes examined. The curve indicates that GT02 performance is again dominant overall. In comparison with SMT, the three tubes have maximum Nusselt number of 42, 35 and 29% for GT02, GT04 and GT06, respectively, at Re 10,000.

4.3 Local Heat Transfer Coefficient

The local heat transfer coefficient was also observed in each tube for determining more insight of the flow. Local heat transfer coefficient in these types of tubes has been discussed by researchers such as Liu and Jensen (2001) and Jasinski (2011), for in-depth knowledge of the phenomena occurring inside the tube. This curve has been plotted along the circumferential length at a particular axial location. In the present case, the curve is plotted at 1.95 m axial location for tubes GT02, GT04 and GT06 and Re 10,000 as shown in Fig. 13.

All the curves show two peaks which indicates high heating zones forming in the corner points of the groove. The layout of curve is asymmetric because of the rotational

Table 4 Dimensional details of groove tubes GT02, GT04 and GT06

Tube	β (°)	Pitch (in)	Pitch (mm)
GT02	23.6	2	51
GT04	12.3	4	102
GT06	8.3	6	152

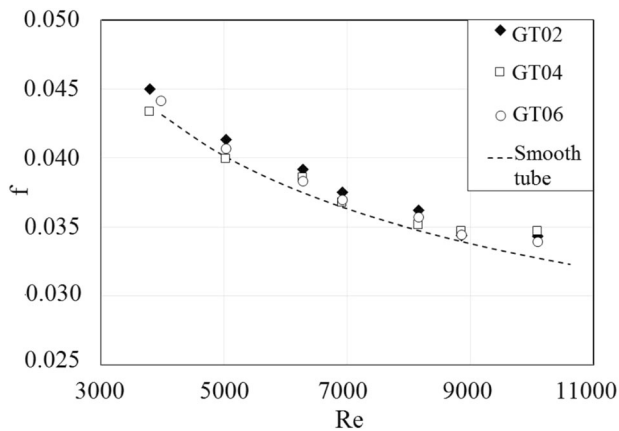


Fig. 11 The friction factor in comparison with smooth tube for groove tubes with 51 mm pitch (GT02), 102 mm pitch (GT04) and 152 mm pitch length (GT06)

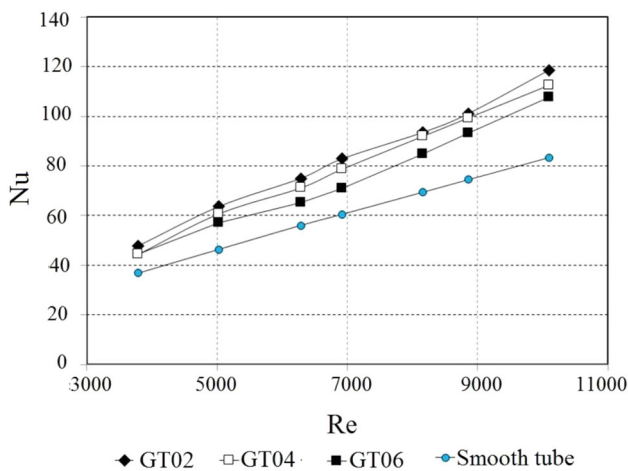


Fig. 12 Nusselt number for groove tubes 51 mm pitch (GT02), 102 mm pitch (GT04) and 150 mm pitch (GT06) and comparison of performance with smooth tube(SMT)

component of flow field due to helix angle. This behavior was also pointed out by Jasinski (2011), where it was also indicated that the asymmetric trend vanishes in case of parallel grooves (grooves aligned with flow direction). Due to its rotational component, when the flow gets separated from surface ‘a’ and strikes the surface ‘b,’ the local heat transfer coefficient in the region increases. The distribution is overall very uniform in the groove-less regions of the tube, i.e., ‘a’ and ‘c.’

4.4 Thermal Enhancement Factor

It is evident that the enhanced area in the tubes due to groove formation will produce turbulence and hence increase the heat transfer. But due to increase in hindrance in the flow, the friction will also increase and hence the pressure drop. Therefore, to incorporate both effects, the

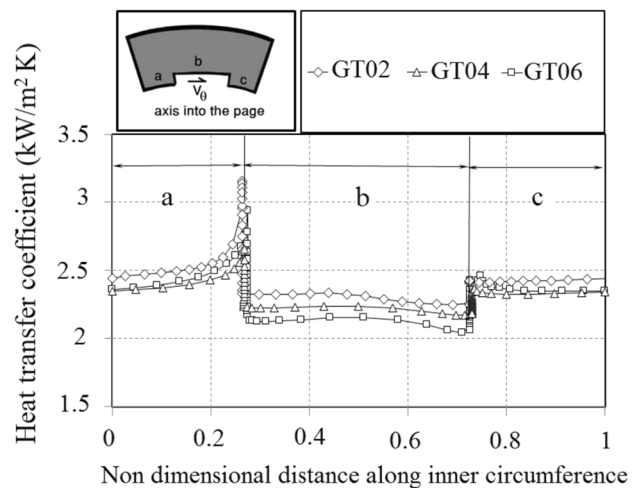


Fig. 13 The local heat transfer coefficient plotted at 1.95 m axial location at $Re = 10,000$ for groove tubes with 51, 102 and 152 mm pitch length

thermal enhancement factor (η) is determined which is the ratio of Nusselt number ratio to the friction factor ratio. The formula is mentioned in Eq. 17.

$$\eta = \frac{Nu/Nu_s}{f/f_s} \tag{17}$$

Figure 14 shows the thermal enhancement factor for groove tubes GT02, GT04 and GT06. The performance is greater than unity, which means that all the grooved designs are capable of enhancing heat transfer relative to the smooth tube. Overall, the above analysis shows GT02 to be the best candidate. It has η 1.25–1.33 over Re range.

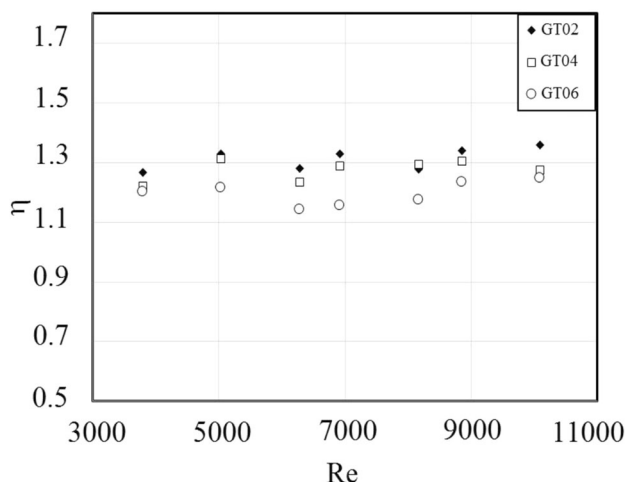


Fig. 14 The thermal enhancement factor for groove tubes with 51, 102 and 152 mm pitch length

5 Conclusion and Future Work

A detailed CFD analysis was performed on helical groove tubes with three geometries from a published article to validate the results, and three other geometries with pitch length apart from experiment. The range of Reynolds number was from 4000 to 10,000.

Results of tubes with pitch length 51, 102 and 152 mm were obtained for friction factor and Nusselt number. Friction factor did not show significant difference in comparison with smooth tube, with maximum of about 5% for GT02 (51 mm pitch length), while Nusselt number showed substantial difference with maximum of 42% for GT02 tube at Re 10,000. The tubes' performance was also compared based on the local heat transfer coefficient showing similar trends of the coefficient among the tubes when plotted along the internal periphery of the tube surface. Lastly, the thermal enhancement factor was analyzed to encounter effects of both friction factor and Nusselt number. The enhancement factor curve showed that GT02 was overall the best candidate among the tubes tested showing maximum of 33% increase in the thermal performance.

Based on the comparison, it can be concluded that GT02 tube or (higher helix angled tube) should be selected, because at the same maximum Reynolds number, it gives the maximum performance. Much lower angled tubes can be tested numerically and will be seen as future objectives. Also, the performance can be further evaluated at much higher Reynolds numbers which is the objective of future research.

Acknowledgements The author would like to acknowledge the institute for providing the computational facility of the PNEC of the National University of Sciences and Technology for performing this work.

References

ANSYS Incorporated (2016) ANSYS Fluent 2016 user guide
Aroonrat K, Jumholkul C, Leelaprachakul R, Dalkilic AS, Mahian O, Wongwises S (2013) Heat transfer and single-phase flow in

- internally grooved tubes. *Int Commun Heat Mass Transf* 42:62–68
- Blasius PR (1913) Das Aehnlichkeitsgesetz bei Reibungsvorgängen in Flüssigkeiten. *Mitteilungen über Forschungsarbeiten auf dem Gebiete des Ingenieurwesens* 131:1–41
- Colebrook CF (1939) Turbulent flow in pipes with particular reference to the transition region between smooth and rough pipe laws. *J Inst Civil Eng* 11:133–156
- Gregory JZ, Chamra MC, Pedro JM (2008) Experimental determination of heat transfer and friction in helically-finned tubes. *Exp Therm Fluid Sci* 32:761–775
- Jamshed S, Qureshi S, Khalid S (2016) Numerical flow analysis and heat transfer in smooth and grooved tubes. In: Brebbia CA (ed) *WIT transactions on engineering sciences. Proceedings of the 11th international conference on engineering sciences (AFM 2016)*, vol 105. WIT Press, Southampton, p 163–174
- Jasinski P (2011) Numerical optimization of flow-heat ducts with helical micro-fins, using entropy generation minimization (EGM) method. In: *Recent advances in fluid mechanics and heat and mass transfer*, Florence, Italy. WSEAS Press, pp 47–54. http://www.wseas.us/e-library/conferences/2011/Florence/HEA_FLU/HEAFLU-04.pdf
- Jensen MK, Vlakancic A (1999) Experimental investigation of turbulent heat transfer and fluid flow in internally finned tubes. *Int J Heat Mass Transf* 42:1343–1351
- Kakaç S, Bergles AE, Mayinger F, Yüncü H (1999) *Heat transfer enhancement of heat exchangers*. Kluwer academic, Dordrecht
- Kim J-H, Jansen KE, Jensen MK (2004a) Analysis of heat transfer characteristics in internally finned tubes. *Numer Heat Transf Part A Appl* 46:21
- Kim J-H, Jansen KE, Jensen MK (2004b) Simulation of three dimensional incompressible turbulent flow inside tubes with helical fins. *Numer Heat Transf Part B Fundam* 46:195–221
- Liu X, Jensen MK (2001) Geometry effects on turbulent flow and heat transfer in internally finned tubes. *J Heat Transf* 123:1035–1044
- Nikuradse J (1933) *Strömungsgesetze in rauhen rohren*. VDI-Forschungsheft, Berlin
- Patankar SV (1980) *Numerical heat transfer and fluid flow*. Series in computational methods in mechanics and thermal sciences. Hemisphere Publishing Corporation, New York
- Pirbastami S, Moujaes SF, Mol SG (2016) Computational fluid dynamics simulation of heat enhancement in internally helical grooved tubes. *Int Commun Heat Mass Transf* 73:25–32
- Webb R, Kim N-H (2005) *Principles of enhanced heat transfer*, 2nd edn. CRC Press, London
- Webb RL, Eckert ERG, Goldstein RJ (1971) Heat transfer and friction factor in tubes with repeated rib roughness. *Int J Heat and Mass Transf* 14:601–607
- Webb RL, Narayanamurthy R, Thors P (2000) Heat transfer and friction characteristics of internal helical-rib roughness. *J Heat Transf* 122:130–142